European Congress on Computational Methods in Applied Sciences and Engineering
ECCOMAS 2004
P. Neittaanmäki, T. Rossi, S. Korotov, E. Oñate, J. Périaux, and D. Knörzer (eds.)
Jyväskylä, 24–28 July 2004

SPECTRAL ANALYSIS OF AN ACOUSTICS-CONVECTION UPSTREAM RESOLUTION ALGORITHM AND APPLICATIONS TO COMPUTATIONAL AERODYNAMICS

Joe Iannelli*

*City University
School of Engineering and Mathematical Sciences
Northampton Square
London EC1V 0HB, UK

Key words: CFD, Characteristics, Multi-dimensional Upwind, Implicit Formulation, Finite Elements, Transonic Flows.

Abstract. *Computational aerodynamics benchmarks have been investigated using an intrinsically infinite directional and multi-dimensional upstream-bias formulation that rests on the mathematics and physics of multi-dimensional acoustics and convection. Based upon characteristic velocities, this formulation introduces the upstream bias directly at the differential equation level, before the spatial discretisation, within a characteristics-bias governing system associated with the Euler and Navier-Stokes equations. Through a decomposition of the Euler flux divergence into multi-dimensional acoustics and convection acoustics components, this characteristics-bias system induces consistent upstream bias along all directions of spatial wave propagation, with anisotropic variable-strength upstreaming that correlates with the spatial distribution of characteristic velocities. A conventional Galerkin finite element discretisation of this system on grids of Lagrange quadrilateral elements directly yields an optimal discretely conservative and multi-dimensional upstream approximation for the Euler and Navier-Stokes equations. Even on relatively coarse grids, this method generates essentially non-oscillatory subsonic, transonic and supersonic aerodynamic-flow solutions that preserve constant total enthalpy for adiabatic flows and mirror reference exact solutions.*

1 INTRODUCTION

This paper provides the second part of a two-part investigation into the development of continuum, i.e. non-discrete, multi-dimensional and infinite-directional characteristics-bias approximations of the Euler and Navier-Stokes equations. The first part [1], also presented at this conference, details the synthesis of an acoustics-convection flux divergence decomposition and applications to the computational investigation of gas dynamic flows. This paper presents the spectral analysis of this formulation and applications to aerodynamic flows.

This two-part presentation expounds the multi-dimensional formulation of the acoustics-convection upstream resolution Euler solver detailed in [2]. Developed for the multi-dimensional Euler and Navier-Stokes equations with general equilibrium equations of state, this formulation develops the upstream-bias approximation directly at the differential equation level, before any discretisation. The formulation results in a "companion" characteristics-bias system that is associated with the governing equations and rests on a decomposition of the multi-dimensional Euler jacobian into acoustics and convection components. This analysis, in particular, reveals that no single decomposition of the Euler flux components themselves can contain separate components that respectively correspond to the physics of multi-dimensional acoustics and convection.

This formulation induces the upstream bias along all flow-field directions of wave propagation and enjoys a consistent theoretical support that rests upon the mathematics and physics of multi-dimensional characteristic wave propagation. The formulation, furthermore, supplies a stable and intrinsically infinite directional upstream-bias that induces minimal diffusion for crisp oblique- shock and naturally incorporates a finite element discretisation with implicit time integration because it is straightforward to determine the required jacobian matrices.

For any Mach number, the characteristics-bias system induces consistent upwinding along all wave-propagation directions along every direction radiating from any flow-field point. The upstream directions are continuously updated and high- rate convergence to machine zero achieved without additional shock-capturing terms, data filtering or loss of essential monotonicity.

The formulation induces an anisotropic variable-strength upstream bias that directly correlates with the multi-dimensional spatial distribution of characteristic velocities. The magnitudes of the associated streamwise and crossflow dissipations remain different from and independent of each other, with crossflow dissipation that decreases for increasing Mach number. In this manner the developed formulation will not generate for increasing Mach number as much crosswind dissipation as induced by an isotropic or direction-split formulation. The magnitude of the induced upstream bias, furthermore, depends on local solution smoothness. Only at solution discontinuities, e.g. a shock wave, is the induced upstreaming commensurate with a fully upwind formulation. In regions of solution continuity, the upwind-bias reduces to a minimum, which corresponds to minimal

induced dissipation.

The operation count for this algorithm is comparable to that of a simple flux vector splitting algorithm. The developments in this study have employed basic Lagrange four-noded cells. To determine the ultimate accuracy of bi-linear approximations of fluxes within four-noded cells, for a computationally efficient implementation, this study employs no MUSCL-type local extrapolation of dependent variables.

This paper is organized in 7 sections. After the introductory remarks in Section 1, Section 2 presents the multi-dimensional non-discrete upstream-bias formulation for the Euler and Navier-Stokes equations. A multi-dimensional characteristics analysis for general equations of state is the subject of Section 3, followed by Section 4, which shows that this formulation is genuinely multi-dimensional. Section 5 summarises the finite element discretisation of the characteristics-bias system. Section 6 discusses the numerical results, with concluding remarks presented in Section 7.

2 NON-DISCRETE UPSTREAM-BIAS APPROXIMATION FOR THE EULER AND NAVIER-STOKES EQUATIONS

As detailed in [1], the non-discrete upstream-bias approximation is developed for the Euler and Navier-Stokes equations. With implied summation on repeated subscript indices, these equations can be abridged as the non-linear parabolic system

$$\frac{\partial q}{\partial t} + \frac{\partial f_j(q)}{\partial x_j} - \frac{\partial f_j^{\nu}}{\partial x_j} = 0 \tag{1}$$

which reduces to the Euler hyperbolic system when the fluid-viscosity flux f_j^{ν} identically vanishes. For three-dimensional formulations, $1 \leq j \leq 3$, while the independent variable $(\boldsymbol{x}, t)$, $\boldsymbol{x} \equiv (x_1, x_2, x_3)$, in (1) varies in the domain $D \equiv \Omega \times [t_o, T]$, $[t_o, T] \in \mathcal{R}^+$, $\Omega \subset \mathcal{R}^n$, with $\mathcal{R}$ denoting the real-number field.

The non-discrete, i.e. continuum or before discretisation, upstream-bias approximation derives from a characteristics-bias integral statement associated with (1). The prototype integral statement is

$$\int_{\widehat{\Omega}} \widehat{w} \left(\frac{\partial q}{\partial t} + \frac{\partial f_j(q)}{\partial x_j} - \frac{\partial f_j^{\nu}}{\partial x_j} \right) d\Omega = 0 \tag{2}$$

which is equivalent to the governing system (1) for arbitrary smooth test functions $\widehat{w}$ with compact support in $\widehat{\Omega}$ and arbitrary subdomains $\widehat{\Omega} \subset \Omega$. The characteristic-bias integral is then defined as

$$\int_{\widehat{\Omega}} \widehat{w} \left(\frac{\partial q}{\partial t} + \frac{\partial f_j^{C}}{\partial x_j} - \frac{\partial f_j^{\nu}}{\partial x_j} \right) d\Omega = 0 \tag{3}$$

where f_j^C corresponds to a characteristics flux that automatically induces within (3) a multi-dimensional and infinite directional upstream-bias approximation for the hyperbolic flux divergence $\frac{\partial f_j}{\partial x_j}$. Most importantly, since the characteristics flux is developed independently and before any discretisation, a genuinely multi-dimensional upstream-bias

approximation for the governing equations (1) on arbitrary grids directly results from a straightforward centered discretisation of the characteristics flux on the given grid.

As detailed in the other paper of this author's at this conference, [1], the acoustics-convection characteristics flux divergence for the Euler and Navier-Stokes system is expressed as

$$\frac{\partial f_j^C}{\partial x_j} = \frac{\partial f_j}{\partial x_j} - \frac{\partial}{\partial x_i}\left[\varepsilon\bar{\psi}\left(c\left(\alpha a_i a_j + \alpha^N a_i^N a_j^N\right)\frac{\partial q}{\partial x_j} + a_i\frac{\partial f_j^q}{\partial x_j} + a_i\delta\frac{\partial f_j^p}{\partial x_j}\right)\right] \tag{4}$$

where f_j^q and f_j^p respectively denote the convection and pressure flux components. For 2-D flows, these components are defined as

$$f_j^q(q) \equiv \begin{Bmatrix} m_j \\ \frac{m_j}{\rho}m_1 \\ \frac{m_j}{\rho}m_2 \\ \frac{m_j}{\rho}(E+p) \end{Bmatrix} = \frac{m_j}{\rho}\cdot\begin{Bmatrix} \rho \\ m_1 \\ m_2 \\ E+p \end{Bmatrix} \quad , \quad f_j^p(q) \equiv \begin{Bmatrix} 0 \\ p\delta_1^j \\ p\delta_2^j \\ 0 \end{Bmatrix} \tag{5}$$

with straightforward generalization to 3-D flows. In the array q, the variables ρ, m_1, m_2 , E, respectively denote static density, volume-specific linear momentum components and total energy, with p and c representing static pressure and speed of sound. The non-negative variables ε, $\bar{\psi}$, α, α^N and δ, of which the magnitude does not exceed one, respectively indicate a reference length, upstream-bias controller, streamwise and cross-flow acoustic upstream functions and pressure-gradient upstream function. The direction cosines a_i, a_i^N, $1 \leq i \leq 2$, respectively correspond to the i^{th} component of unit vectors parallel and perpendicular to the local velocity vector. In result (4), the expressions $\left(c\alpha a_i a_j\frac{\partial q}{\partial x_j} + a_i\frac{\partial f_j^q}{\partial x_j} + a_i\delta\frac{\partial f_j^p}{\partial x_j}\right)$ and $\left(c\alpha^N a_i^N a_j^N\frac{\partial q}{\partial x_j}\right)$ determine the upstream biases within respectively the streamline and crossflow wave propagation regions.

3 CHARACTERISTICS ANALYSIS

Within a 2-D flow field, acoustic and convection waves propagate in infinitely many directions, on the flow plane, and along each direction the associated propagation velocity also depends on the Mach number. This section presents an intrinsically multi-dimensional characteristics analysis based on non-linear wave-like solutions. This analysis leads to the spatial distribution of multi-dimensional propagation velocities and shows that among all propagation directions the streamline and crossflow directions are principal propagation directions. This line of enquiry yields specific conditions for a physically coherent upstream bias formulation that remains consistent with multi-dimensional acoustic and convection wave propagation.

3.1 Characteristic Velocity Components

The non-linear wave-like form of q is expressed as

$$q = q(\eta_1) \quad , \quad \eta_1 = \boldsymbol{x} \cdot \boldsymbol{n} - \lambda(q)t = x_j n_j - \lambda(q)t \tag{6}$$

where $\boldsymbol{n}$ denotes a space-domain propagation-direction unit vector, independent of $(\boldsymbol{x}, t)$, and $\lambda = \lambda(q)$ indicates a wave-propagation velocity component along the $\boldsymbol{n}$ direction. This solution-dependent velocity component is determined by enforcing the condition that the non-linear wave-like solution (6) satisfies the Euler equations. This condition yields the eigenvalue problem

$$\left(-\lambda(q)I + \frac{\partial f_j}{\partial q} n_j\right) \frac{\partial q}{\partial \eta_1} = 0 \tag{7}$$

For non-trivial solutions $\frac{\partial q}{\partial \eta_1}$, hence $q = q(\eta_1)$, the characteristic velocity components λ are

$$\lambda_{1,2}^{d_E} = u_j n_j \quad , \quad \lambda_{3,4}^{d_E} = u_j n_j \pm c \tag{8}$$

where superscript d_E signifies dimensional Euler eigenvalues. The non-dimensional form of (8) follows from division by c, which supplies the Mach-number dependent expressions

$$\lambda_{1,2}^{E} = v_j n_j M \quad , \quad \lambda_{3,4}^{E} = v_j n_j M \pm 1 \tag{9}$$

where v_1 and v_2 denote the components of a unit vector $\boldsymbol{v}$ in the velocity $\boldsymbol{u}$ direction.

As the inner product of the two unit vectors $\boldsymbol{n}$ and $\boldsymbol{v}$, the contraction $v_j n_j$ supplies the cosine of the angle $(\theta - \theta_{\boldsymbol{v}})$ between $\boldsymbol{n}$ and $\boldsymbol{v}$, where θ and $\theta_{\boldsymbol{v}}$ respectively denotes the angle between $\boldsymbol{n}$ and the x_1 axis and the angle between $\boldsymbol{v}$ and the x_1 axis. The eigenvalues (9) thus become

$$\lambda_{1,2}^{E} = \cos(\theta - \theta_{\boldsymbol{v}})\, M \quad , \quad \lambda_{3,4}^{E} = \cos(\theta - \theta_{\boldsymbol{v}})\, M \pm 1 \tag{10}$$

These expressions, in particular, imply that the Euler eigenvalues achieve their extrema for $\theta = \theta_{\boldsymbol{v}}$, hence when $\boldsymbol{n}$ points in the streamline direction, whereas for $\boldsymbol{n}$ pointing in the crossflow direction, hence $\theta = 90^o + \theta_{\boldsymbol{v}}$, these eigenvalues no longer depend upon M.

The convection eigenvalues $\lambda_{1,2}^{E}$ vanish when $\cos(\theta - \theta_{\boldsymbol{v}}) = 0$, hence for $\boldsymbol{n}$ perpendicular to the streamline direction, or, equivalently, pointing in the crossflow direction. Since $\| \cos(\theta - \theta_{\boldsymbol{v}}) \| \leq 1$, the acoustic-convection eigenvalues $\lambda_{3,4}^{E}$ can only vanish for $M \geq 1$, hence for supersonic flows. For these flows, $\lambda_{3,4}^{E} = 0$ for

$$\mp \cos(\theta - \theta_{\boldsymbol{v}}) = \pm \sin((\theta - 90^o) - \theta_{\boldsymbol{v}}) = \frac{1}{M} \tag{11}$$

hence for $\boldsymbol{n}$ perpendicular to the Mach lines, for $\pm((\theta - 90^o) - \theta_{\boldsymbol{v}})$ corresponds to the angle between a Mach line and the streamline, from the well known second expression in (11). The lines that are perpendicular to the Mach lines will be called "conjugate" lines.

The lines that are perpendicular to $\boldsymbol{n}$ for vanishing eigenvalues $\lambda^E_{1,2}$ and $\lambda^E_{3,4}$ thus respectively become the streamline and Mach lines. This result is not coincidental, for vanishing eigenvalues $\lambda^E_{1,4}$ correspond to wave-like solutions of the steady Euler equations, for which the streamline and Mach lines are characteristic-wave propagation lines.

3.2 Polar Variation of Characteristic Speeds

Figure 1 presents the polar variation of the absolute values of eigenvalues (9) for subsonic, sonic and supersonic Mach numbers, in a neighborhood of a flow field point P in the (x_1, x_2) plane. These variations are obtained for a variable unit vector $\boldsymbol{n} \equiv (\cos\theta, \sin\theta)$ and fixed unit vector $\boldsymbol{v}$, in this representative case inclined by $+30^o$ with respect to the x_1 axis,

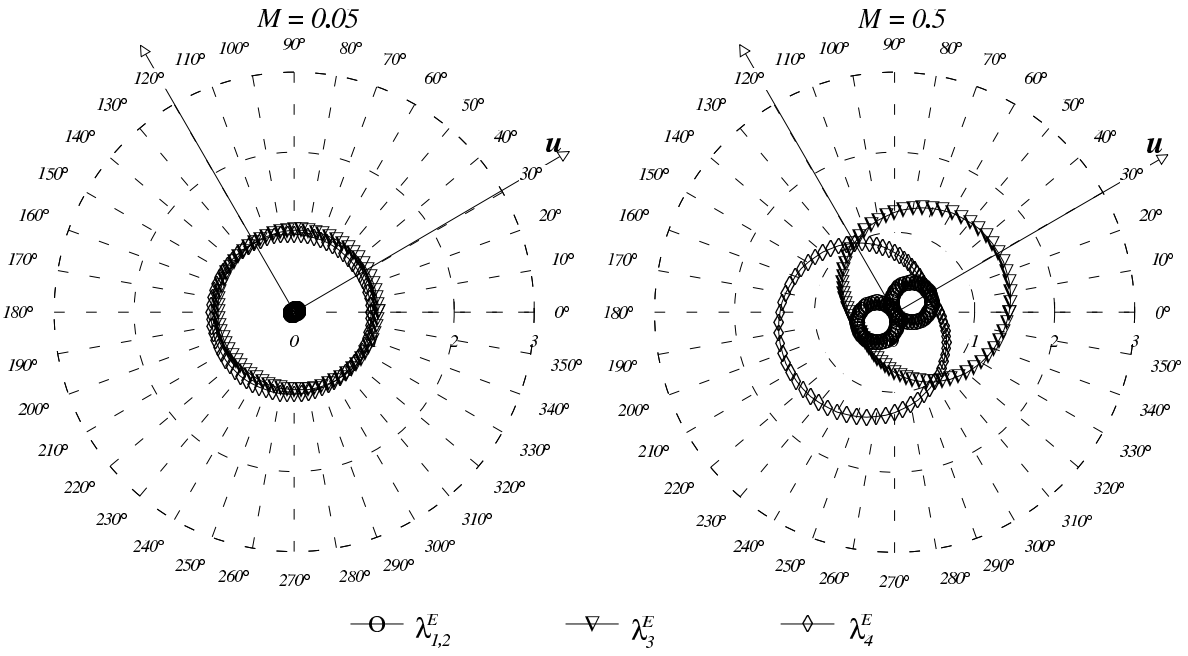

Figure 1: Polar Variation of Subsonic Wave Speeds

A collective inspection of all these diagrams reveals three shared features for all Mach numbers. The maximum characteristic speeds occur in the velocity direction, i.e. along a streamline, as noted before. Secondly, all the characteristic speeds are symmetrically distributed about the streamline direction. Thirdly, the eigenvalue pairs $(\|\lambda^E_1\|, \|\lambda^E_2\|)$ and $(\|\lambda^E_3\|, \|\lambda^E_4\|)$ remain mirror skew-symmetric with respect to the crossflow direction,

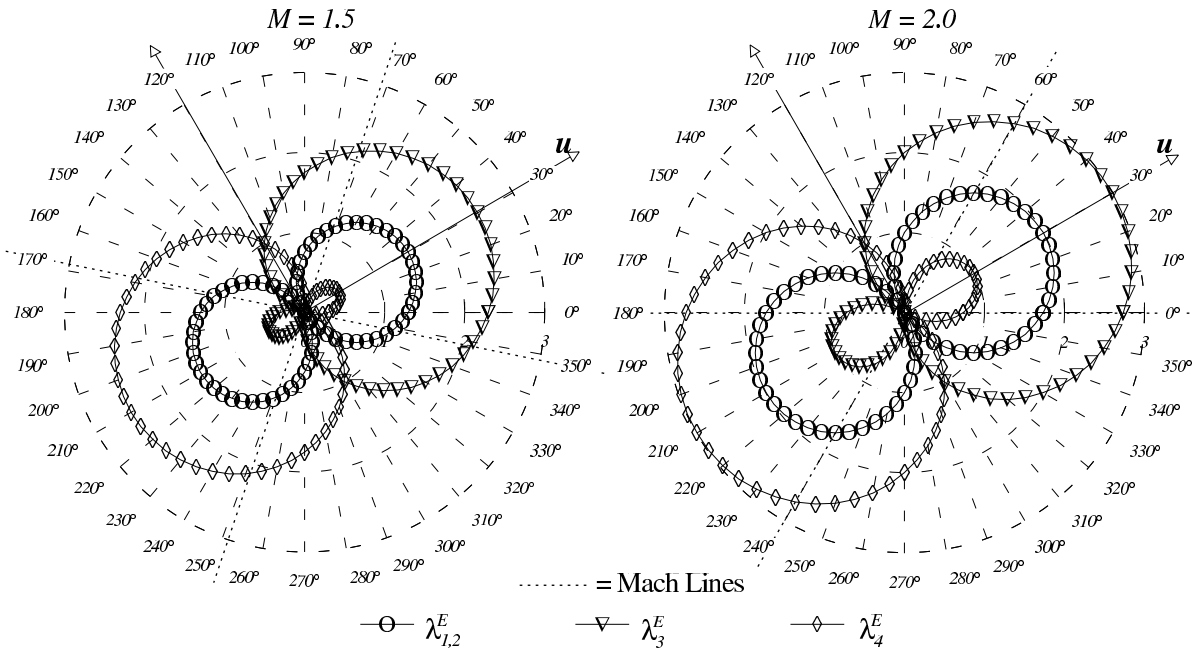

Figure 2: Polar Variation of Supersonic Wave Speeds

in the sense that the curves representative of $\|\lambda_2^E\|$ and $\|\lambda_4^E\|$ become the respective mirror images of the variations of $\|\lambda_1^E\|$ and $\|\lambda_3^E\|$ with reference to this direction. The streamline and crossflow directions, therefore, become two fundamental wave-propagation axes.

For vanishing Mach numbers, the acoustic-convection propagation curves in the figure approach two circumferences. The distribution of propagation speeds in this case is therefore isotropic, which corresponds to the direction-invariant propagation of acoustic waves. As the Mach number increases from zero, the curves in the figure progressively become circular asymmetric, which corresponds to anisotropic wave propagation. For $M = 0.5$ this anisotropy is already evident and becomes more pronounced for higher Mach numbers. The non-dimensional characteristic speeds then approach 1 in the region about the crossflow direction, which corresponds to essentially acoustic propagation.

For all Mach numbers, the convection eigenvalues $\lambda_{1,2}$ change sign when the $\boldsymbol{n}$-direction shifts from an upstream to a downstream axis with respect to $\boldsymbol{u}$. For this reason, the associated curves cross the polar origin. Pure convective propagation, therefore, remains mono-axial, from upstream to downstream of P, and the axis of this type of wave propagation is the streamline.

For subsonic Mach numbers the acoustic-convection eigenvalues λ_3^E and λ_4^E respectively remain positive and negative for all directions. For this reason the associated curves contain the polar origin. For subsonic flows, therefore, acoustic-convection waves propagate bi-modally, from both upstream and downstream toward and away from point P, along

all directions radiating from P.

Beginning at the sonic state, this pattern drastically changes for supersonic Mach numbers. In this case both λ_3^E and λ_4^E change algebraic sign when the $\boldsymbol{n}$ shifts from upstream to downstream of P along a streamline. For this reason, the associated curves cross the polar origin. For supersonic flows, therefore, acoustic-convection wave propagation becomes mono-axial along a streamline, from upstream to downstream of P.

4 INFINITE DIRECTIONAL UPSTREAM BIAS

In jacobian form, expression (4) becomes

$$\frac{\partial f_j^C}{\partial x_j} = \frac{\partial f_j}{\partial x_j} - \frac{\partial}{\partial x_i}\left[\varepsilon\psi\left(c\left(\alpha a_i a_j + \alpha^N a_i^N a_j^N\right) I + a_i \frac{\partial f_j^q}{\partial q} + a_i \delta \frac{\partial f_j^p}{\partial q}\right)\frac{\partial q}{\partial x_j}\right] \tag{12}$$

For 2-D flows, expression (4) and this upstream-bias expression essentially depend upon the five upstream-bias functions $a_1, a_2, \alpha, \delta, \alpha^N$. In order to ensure physical consistency, these functions are determined by imposing on (12) the stringent stability requirement that it should induce an upstream-bias diffusion not just along the principal streamline and crossflow upstream directions, but along all directions $\boldsymbol{n} = (n_1, n_2)$ radiating from any flow-field point. This demanding stability conditions is satisfied when all the eigenvalues of the associated upstream-bias matrix

$$\mathcal{A} \equiv n_i \left(c\left(\alpha a_i a_j + \alpha^N a_i^N a_j^N\right) I + a_i \frac{\partial f_j^q}{\partial q} + a_i \delta \frac{\partial f_j^p}{\partial q}\right) n_j \tag{13}$$

remain positive for all M and propagation directions $\boldsymbol{n}$.

Despite the formidable non-linear algebraic complexity of $\mathcal{A}$, all of its eigenvalues have been analytically determined exactly in closed form. Dividing through the speed of sound c, the non-dimensional form of these eigenvalues is

$$\lambda_{1,2} = n_i\left(\alpha a_i a_j + \alpha^N a_i^N a_j^N\right) n_j + n_i a_i v_j n_j M$$

$$\lambda_{3,4} = n_i\left(\alpha a_i a_j + \alpha^N a_i^N a_j^N\right) n_j + n_i a_i \left(1 + \frac{1-\delta}{2} p_{_E}\right) v_j n_j M \pm n_i a_i \sqrt{\left(\frac{1-\delta}{2} p_{_E} v_j n_j M\right)^2 + \delta} \tag{14}$$

where v_j denotes the j^{th} direction cosine of a unit vector $\boldsymbol{v}$ parallel to the local velocity $\boldsymbol{u}$. Heed that for both $\boldsymbol{a} = \boldsymbol{v}$ and $\boldsymbol{n} = \boldsymbol{v}$, the functions α and δ within (14) determine the corresponding streamline upstream-bias eigenvalues

$$\lambda_{1,2} = \alpha + M \quad , \quad \lambda_{3,4} = \alpha + \left(1 + \frac{1-\delta}{2} p_{_E}\right) M \pm \sqrt{\left(\frac{1-\delta}{2} p_{_E} M\right)^2 + \delta} \tag{15}$$

Rather than prescribing some expressions for α and δ and accepting the resulting variations for these eigenvalues, physically consistent expressions for the streamline upstream-bias eigenvalues are instead prescribed and the corresponding functions for α and δ determined.

4.1 Conditions on Upstream-Bias Functions and Eigenvalues

The eigenvalues (14) are expressed as

$$\lambda_{1,4} = \lambda_{1,4}\left(M, \boldsymbol{n}\right) \tag{16}$$

to stress their dependence upon both M and $\boldsymbol{n}$. The five conditions for the determination of the five functions $a_1, a_2, \alpha, \delta, \alpha^N$ are

$$a_1^2 + a_2^2 = 1, \quad \lambda_{1,2}\left(M, \boldsymbol{n}\right) \geq 0, \quad \lambda_1\left(M, \boldsymbol{v}\right) = \lambda_1, \quad \lambda_4\left(M, \boldsymbol{v}\right) = \lambda_4, \quad \lambda_{3,4}\left(M, \boldsymbol{n}\right) \geq 0 \tag{17}$$

where λ_1 and λ_4 now denote prescribed streamline upstream-bias eigenvalues. The first condition stipulates $\boldsymbol{a}$ as a unit vector and with the second condition it determines both $\boldsymbol{a}$ and $\boldsymbol{a}^N$, for $\boldsymbol{a}$ and $\boldsymbol{a}^N$ are mutually perpendicular. In particular, these two conditions theoretically confirm that the unit vectors $\boldsymbol{a}$ and $\boldsymbol{a}^N$ respectively point along the streamline and crossflow directions. The third and fourth conditions stipulate that the streamline upstream-bias eigenvalues must equal prescribed eigenvalues, which leads to α and δ. For the determined $\boldsymbol{a}$, $\boldsymbol{a}^N$, α and δ, the fifth condition then establishes α^N.

4.2 Streamline Eigenvalue λ_4

This eigenvalue will correlate with the absolute Euler eigenvalue $|M-1|$. As a consequence, λ_4 will vary between 1 and $1-M$ for $0 \leq M \leq 1-\varepsilon_M$ and smoothly shift from $1-M$ to $M-1$ within the sonic transition layer $1-\varepsilon_M \leq M \leq 1+\varepsilon_M$, where ε_M denotes a transition-layer parameter; in this work $\varepsilon_M = \frac{1}{5}$. One expression for λ_4 that remains smooth and meets these requirements is the composite spline

$$\lambda_4(M) \equiv \begin{cases} 1-M & , \quad 0 \leq M \leq 1-\varepsilon_M \\ \dfrac{(M-1)^2}{2\varepsilon_M} + \dfrac{\varepsilon_M}{2} & , \quad 1-\varepsilon_M < M < 1+\varepsilon_M \\ M-1 & , \quad 1+\varepsilon_M \leq M \end{cases} \tag{18}$$

4.3 Streamline Eigenvalue λ_1

This eigenvalue correlates with the non-dimensional Euler eigenvalue M, but it too has to equal 1 for $M = 0$; it then must coincide with M for $M > 1$ and also remain greater than λ_4, as expressed through (18), for consistency with the Euler eigenvalues (8). This condition in particular implies $\lambda_1 \geq \frac{1}{2}$. It thus follows that λ_1 will vary between 1 and M for $0 \leq M \leq \frac{1}{2} + \varepsilon_M$. An expression for $\lambda_1 = \lambda_1(M)$ that remains smooth and meets all

of these requirements is the composite spline

$$\lambda_1(M) \equiv \begin{cases} 1-M & , \quad 0 \leq M \leq \frac{1}{2}-\varepsilon_M \\ \dfrac{(M-\frac{1}{2})^2}{2\varepsilon_M}+\dfrac{1+\varepsilon_M}{2} & , \quad \frac{1}{2}-\varepsilon_M < M < \frac{1}{2}+\varepsilon_M \\ M & , \quad \frac{1}{2}+\varepsilon_M \leq M \end{cases} \tag{19}$$

4.4 Upstream-Bias Functions a, α, δ and α^N

These functions are used in actual computations based on the characteristics flux divergence (4). In the eigenvalues $\lambda_{1,2}$ in (14), the components

$$n_i \alpha a_i a_j n_j = \alpha \left(a_j n_j\right)^2 \quad , \quad n_i \alpha^N a_i^N a_j^N n_j = \alpha^N \left(a_j^N n_j\right)^2 \tag{20}$$

are already non-negative for non-negative α and α^N. The eigenvalues $\lambda_{1,2}$, therefore, will remain non-negative for all positive α and α^N, including $\alpha \to 0$ and $\alpha^N \to 0$, when the additional component $n_i a_i v_j n_j M$ remains non-negative for all M. This requirement is met along with the first condition in (17) when $\boldsymbol{a} = \boldsymbol{v}$, for

$$n_i a_i v_j n_j M = M \left(v_j n_j\right)^2 \geq 0 \tag{21}$$

This finding is not surprising, for the streamline direction is a (principal) characteristic direction.

From λ_1 and λ_4 in (15), the corresponding expressions for both $\alpha = \alpha(M)$ and $\delta = \delta(M)$ are then directly and exactly determined as

$$\alpha(M) = \lambda_1(M) - M \quad , \quad \delta(M) = \frac{\left(\lambda_1(M) - \lambda_4(M)\right)\left(\lambda_1(M) - \lambda_4(M) + p_{_E} M\right)}{1 + p_{_E} M \left(\lambda_1(M) - \lambda_4(M)\right)} \tag{22}$$

where according to the third and fourth conditions in (17) the streamline eigenvalues λ_4 and λ_1 are respectively given by (18), (19).

With $M_M = 1 + \epsilon_M$, the fifth condition in (17) leads to the following expression for α^N

$$\alpha^N(M) \equiv \begin{cases} 1 + \left(\dfrac{3(\alpha^N(M_M)-1)}{M_M^2} - \dfrac{\alpha^{N\prime}(M_M)}{M_M}\right) M^2 + \left(\dfrac{\alpha^{N\prime}(M_M)}{M_M^2} - \dfrac{2(\alpha^N(M_M)-1)}{M_M^3}\right) M^3, \\ \qquad 0 \leq M < M_M \\ \dfrac{1}{2}\left(1 + \dfrac{\varepsilon_M}{M_M - \sqrt{M_M^2-1}}\right)\left(M - \sqrt{M^2-1}\right) \quad , \quad M_M \leq M \end{cases} \tag{23}$$

where superscript prime "$\prime$" denotes differentiation with respect to M.

4.5 Polar Variation of Upstream-Bias

The directional variation of the upstream bias eigenvalues (14) is presented in Figures 3 - 4 for representative subsonic and supersonic Mach numbers. These variations are obtained for a variable unit vector $\boldsymbol{n} \equiv (\cos\theta, \sin\theta)$ and fixed unit vector $\boldsymbol{a} = \boldsymbol{v}$, in this representative case inclined by $+30^o$ with respect to the x_1 axis.

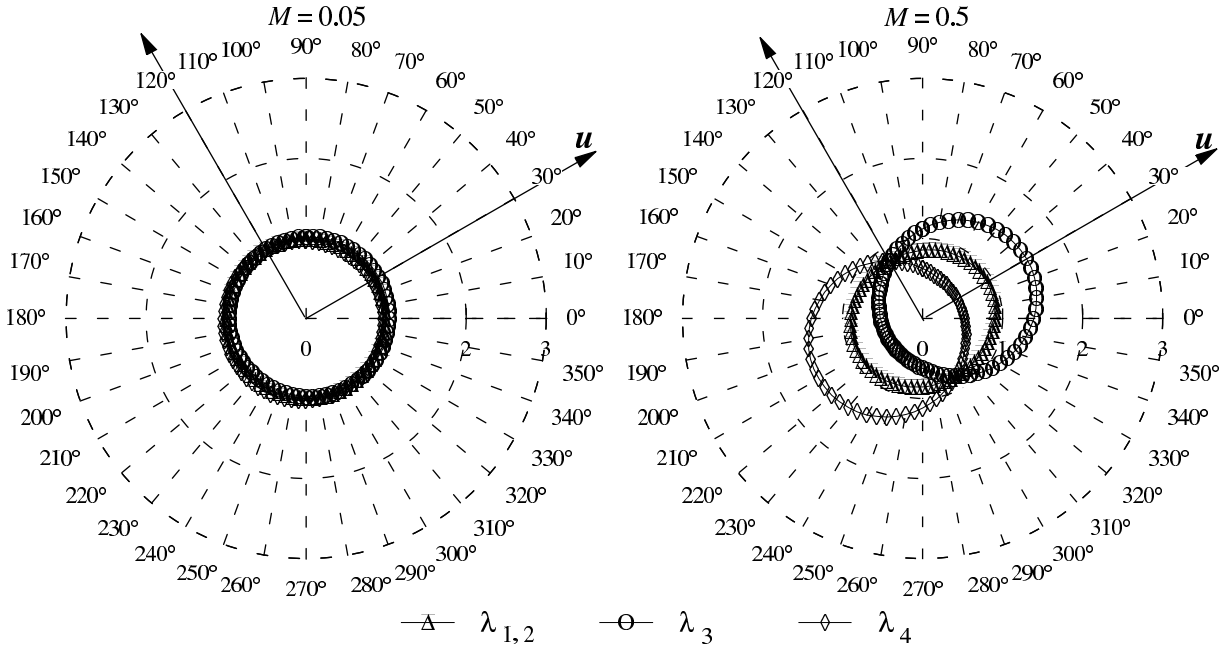

Figure 3: Polar Variation of Subsonic Upstream Bias

These figures collectively indicate that the characteristics flux divergence (4) induces a physically consistent upstream bias because for any Mach number and wave propagation direction $\boldsymbol{n}$ the associated upstream-bias eigenvalues (14) remain positive and their directional variation mirrors the directional variation of the characteristic Euler eigenvalues (8). The upstream-bias eigenvalues, moreover, are symmetrical about the crossflow direction and characteristic streamline, precisely like the characteristic Euler eigenvalues. For $M = 0.05$, the directional variation of the upstream-bias eigenvalues in Figure 3 correlates with that in Figure 1 and thereby corresponds to an isotropic upstream bias, in complete agreement with the isotropic acoustic wave propagation speed in the Euler equations. For increasing Mach numbers, the upstream bias becomes anisotropic, again in agreement with the anisotropic distribution of the Euler eigenvalues (8). For $M = 0.5$ this anisotropy is already evident and then becomes more marked for supersonic Mach numbers as indicated in Figure 4. In particular, the crossflow upstream bias decreases for increasing Mach number.

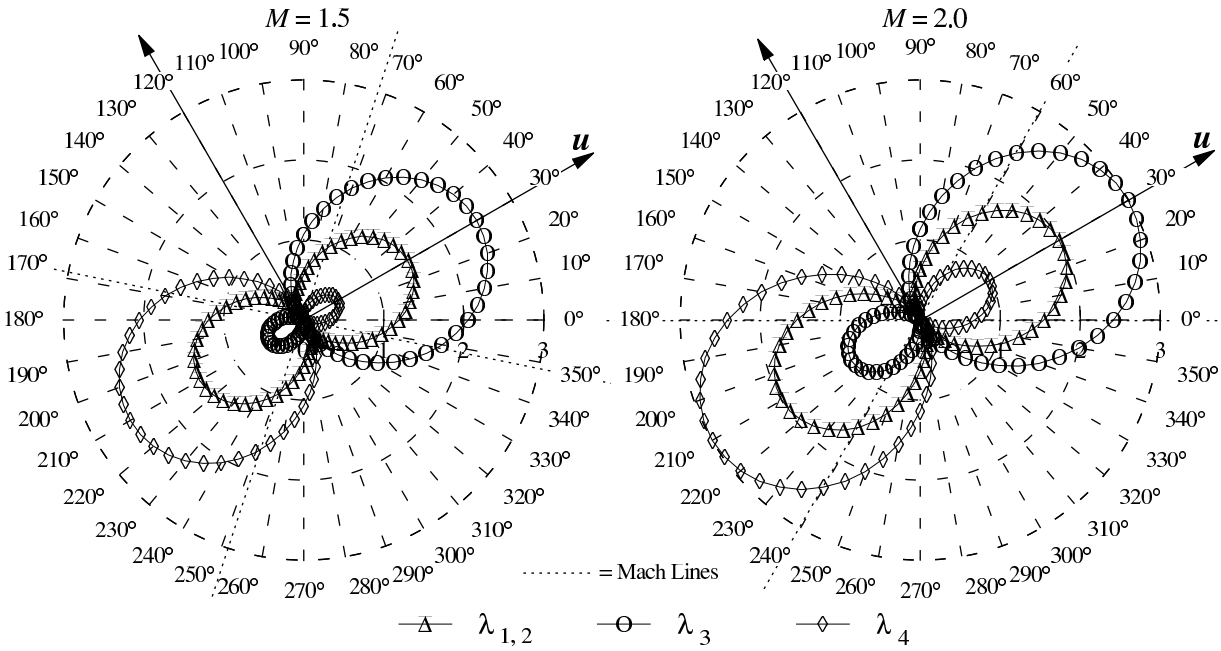

Figure 4: Polar Variation of Supersonic Upstream Bias

Figures 5 - 6 compare the directional variations of the representative upstream-bias eigenvalue λ_3 and the corresponding Euler eigenvalue λ_3^E. This comparison is sufficient to depict the correlation between all the Euler and upstream-bias eigenvalues, for $\lambda_{1,2}$ and $\lambda_{1,2}^E$ are topologically similar to each other, compare Figures 2 and 4, while λ_4 and λ_4^E are respectively mirror skew-symmetric to λ_3 and λ_3^E with respect to the crossflow direction.

As Figures 5 - 6 indicate, λ_3 is symmetrical about the characteristic streamline, precisely like the corresponding characteristic Euler eigenvalue λ_3^E and the corresponding polar curve is topologically similar to the Euler eigenvalue curve. For $M = 0.05$, λ_3 and λ_3^E virtually coincide with each other and remain direction invariant, which corresponds to an isotropic upstream bias in correlation with the acoustic speed. For $M = 0.5$, Figure 5 indicates that λ_3^E is greater than λ_3 in the streamline direction.

For supersonic Mach numbers, λ_3 in the streamline direction coincides with $M + 1$. As shown in Figure 6, therefore, the magnitude of the upstream bias for supersonic flows is virtually identical to the magnitude of the characteristic eigenvalues, within the domain of dependence and range of influence of any flow field point. Outside this region, the upstream-bias eigenvalues are modestly less than the characteristic eigenvalues. In these variations, the upstream-bias eigenvalues are vanishingly small in the cross- flow direction, which, in particular, corresponds to minimal crossflow diffusion.

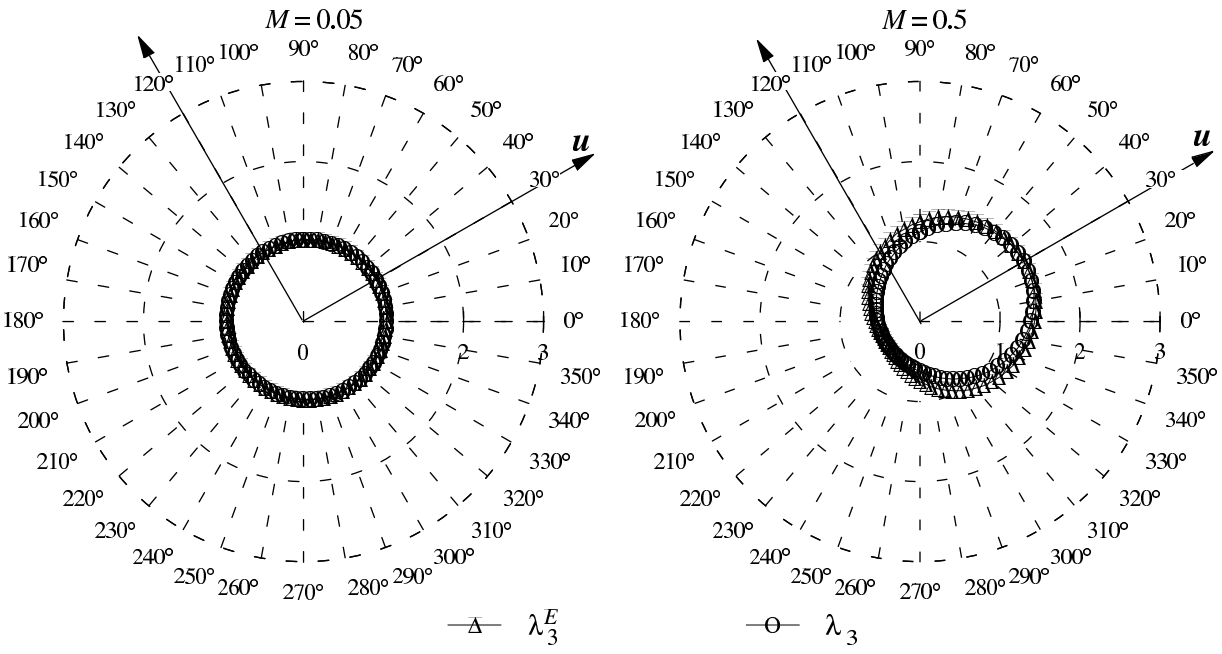

Figure 5: Polar Correlation of Subsonic Characteristic λ_3^E and Upstream λ_3

5 FINITE ELEMENT WEAK STATEMENT

The divergence (4) of the characteristics flux f_j^C leads to the following characteristics-bias integral statement with implied summation on repeated subscript indices i, j

$$\int_\Omega w \left[\frac{\partial q}{\partial t} + \frac{\partial f_j}{\partial x_j} - \frac{\partial}{\partial x_i} \left(\varepsilon \bar{\psi} \left(c \left(\alpha a_i a_j + \alpha^N a_i^N a_j^N \right) \frac{\partial q}{\partial x_j} + a_i \frac{\partial f_j^q}{\partial x_j} + a_i \delta \frac{\partial f_j^p}{\partial x_j} \right) \right) \right] d\Omega = 0 \tag{24}$$

An integration by parts of the characteristics-bias expression then generates the weak statement

$$\int_\Omega \left[w \left(\frac{\partial q}{\partial t} + \frac{\partial f_j}{\partial x_j} \right) + \frac{\partial w}{\partial x_i} \varepsilon \bar{\psi} \left(c \left(\alpha a_i a_j + \alpha^N a_i^N a_j^N \right) \frac{\partial q}{\partial x_j} + a_i \frac{\partial f_j^q}{\partial x_j} + a_i \delta \frac{\partial f_j^p}{\partial x_j} \right) \right] d\Omega = 0 \tag{25}$$

where the surface integral on $\partial\Omega$ corresponding to the characteristics-bias expression vanishes because of the boundary condition $\bar{\psi}(\boldsymbol{x}_{\partial\Omega}) = 0$, imposed to eliminate unnecessary boundary upstream bias. The discrete equations then result from a finite element discretisation of this weak statement. An analogous statement applies to the Navier-Stokes equations.

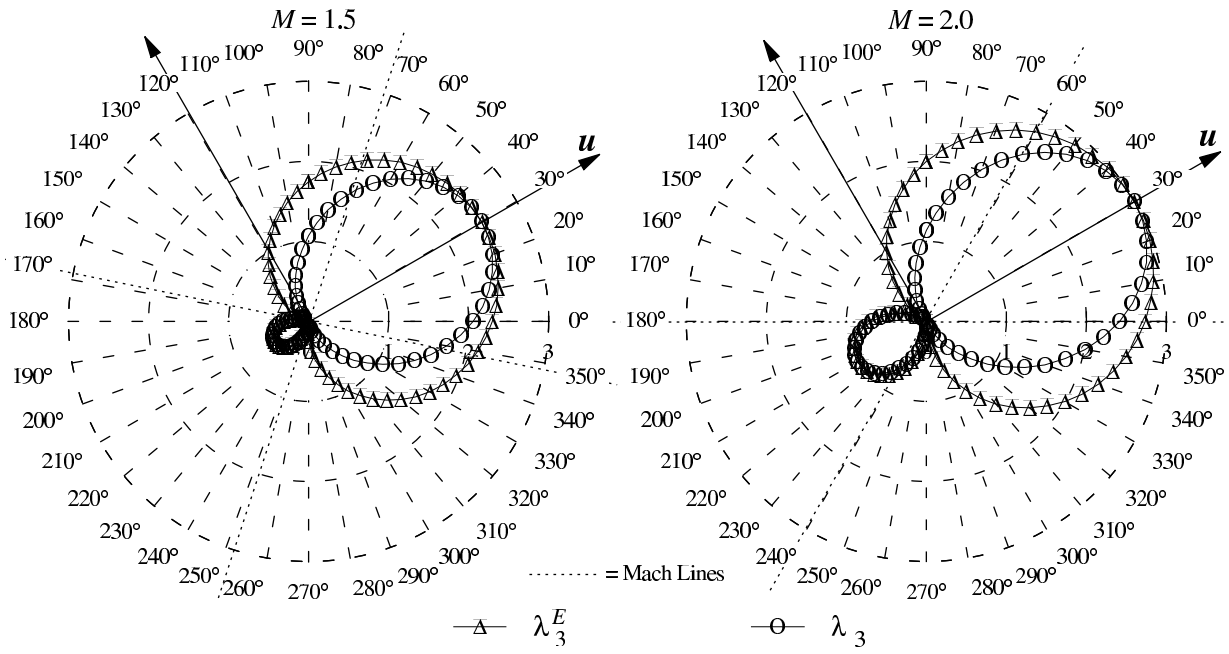

Figure 6: Polar Correlation of Supersonic Characteristic λ_3^E and Upstream λ_3

The finite element weak statement associated with (25) is

$$\int_{\Omega^h} w^h \left(\frac{\partial q^h}{\partial t} + \frac{\partial f_j^h}{\partial x_j} \right) d\Omega +$$

$$+ \int_{\Omega^h} \frac{\partial w^h}{\partial x_i} \varepsilon^h \overline{\psi}^h \left(c^h \left(\alpha^h a_i^h a_j^h + \alpha^{N^h} a_i^{N^h} a_j^{N^h} \right) \frac{\partial q^h}{\partial x_j} + a_i^h \frac{\partial f_j^{q^h}}{\partial x_j} + a_i^h \delta^h \frac{\partial f_j^{p^h}}{\partial x_j} \right) d\Omega = 0 \quad (26)$$

where superscript "h" signifies spatial discrete approximation. The approximation q^h exists on a partition Ω^h, $\Omega^h \subseteq \Omega$, of Ω. This partition Ω^h has its boundary nodes on the boundary $\partial\Omega$ of Ω and results from the union of N_e non-overlapping elements Ω_e, $\Omega^h = \bigcup_{e=1}^{N_e} \Omega_e$. Within Ω^h, there exists a cluster of "master" elements Ω_k^M, each comprising only those adjacent elements that share a mesh node $\boldsymbol{x}_k$, with $1 \leq k \leq N$, where N denotes the total number of mesh nodes and hence master elements.

The discrete test function w^h within each master element Ω_k^M will coincide with the "pyramid" basis function $w_k = w_k(\boldsymbol{x})$, $1 \leq k \leq N$, with compact support on Ω_k^M. Such a function equals one at node $\boldsymbol{x}_k$, zero at all other mesh nodes and also identically vanishes both on the boundary segments of Ω_k^M not containing $\boldsymbol{x}_k$ and on the computational domain outside Ω_k^M.

In this study, each of the variables $\overline{\psi}^h$, α^h, c^h, $\boldsymbol{a}^h$, $\boldsymbol{a}^{N^h}$ and δ^h has been set equal to a piece wise constant for computational simplicity, one centroidal constant value per

element. Likewise, ε^h is set equal to a reference length within each element, typically a measure of the element size. In this study, $\varepsilon^h = (\ell)_e/2$ within each element "e", where $(\ell)_e$ denotes the length of the streamline diameter of the generalized ellipse inscribed within the element. The choice of a diameter in the streamline direction for $(\ell)_e$ rests on the recognition that the streamline is a characteristic principal direction, as discussed in Sections 3.2-3.3.

Since the test and trial functions w_ℓ are prescribed functions of $\boldsymbol{x}$, the spatial integrations in (26) are directly carried out. For arbitrarily shaped elements, these integrations take place via the usual finite element local-coordinate transformation that for example maps a quadrilateral into a square. In this study, the resulting coordinate- transformation metrics within each element are set to constants equal to their respective centroidal values. This simplification allows the exact integration of the remaining integrals, which are then evaluated only once for each computation. Concerning the boundary variables, no extrapolation of variables is needed in this algorithm on a variable that is not constrained via a Dirichlet boundary condition. In this case, instead, the finite element algorithm (26) naturally generates for each unconstrained boundary variable a boundary-node ordinary differential equation. The complete integration with respect to $\boldsymbol{x}$ transforms (26) into a system of continuum-time ordinary differential equations (ODE) for determining at each time level t the unknown nodal values $q^h(\boldsymbol{x}_\ell, t)$, $1 \leq \ell \leq N$. This ODE system is numerically integrated in time via an implicit diagonal Runge-Kutta algorithm that remains absolutely stable for stiff non-linear dissipative systems, [2, 21]. The resulting linear algebra problems are then solved through Gaussian elimination and GMRES.

6 Computational Results

The Acoustics-Convection Upstream Resolution Algorithm has generated essentially non-oscillatory results, as exemplified by solutions for a 2-D transonic flow about a 3% thick symmetrical aerofoil. The subsonic inlet corresponds to a free-stream Mach number $M_\infty = 0.87$, hence the inlet boundary conditions only constrain density ρ, transverse linear momentum component m_2 and total energy E. The outlet, consisting of both the downstream exit and upper side, remains subsonic, hence static pressure is constrained at this boundary. At the lower streamline, the inviscid wall-tangency boundary condition is enforced. A pressure drop is imposed upon an initially quiescent field and the final steady state is computationally achieved by advancing the solution in time.

The finite element discretisation has employed Lagrange bilinear elements and the computational efficiency of the procedure has remained comparable to that of a conventional centered algorithm for the characteristics-bias system. As shown in Figure 7, the computational solution corresponds to a relatively coarse body -fitted grid of 40 bilinear elements in the transverse and longitudinal directions, for a total of 1600 elements, 1681 nodes and 6724 degrees of freedom. The upstream directions were continuously updated without any filtering or freezing, with high-rate convergence of the residual norm to 1×10^{-14}, hence machine zero, achieved in less than 50 time cycles at a constant maximum Courant

number in excess of 100. The Mach-number flooded contours in the figure reveal the

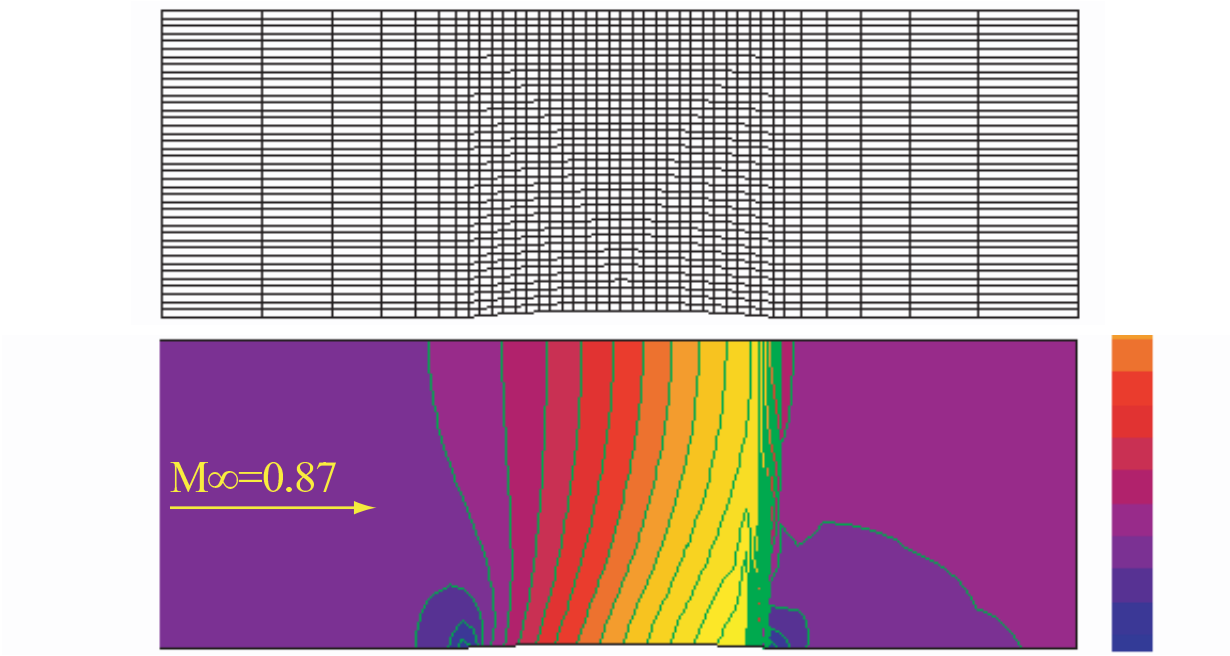

Figure 7: $M_\infty = 0.87$ Aerofoil Transonic Flow, Computational Grid, Mach Number Field

development of a supersonic pocket terminated by a sharp shock adjacent to the aerofoil trailing edge. Figure 8 presents the Mach-number distribution. This distribution portrays a non-oscillatory solution with crisply captured shock and compressions and expansions at the aerofoil leading and trailing edges. Significantly, the calculated total enthalpy remains essentially constant throughout the field and additional solutions calculated on progressively refined grids confirmed the accuracy of the solution. Additional results are presented at the conference.

7 CONCLUDING REMARKS

The characteristics-bias upstream formulation rests upon the physics and mathematics of multi - dimensional characteristic acoustics and convection for general equations of state. It generates the upstream bias at the differential equation level, before any discrete approximation, by way of a characteristics-bias system and associated decomposition of the Euler flux divergence into convection and streamline and crossflow acoustic components.

A natural finite element discretisation of the characteristics-bias system directly provides a genuinely multi-dimensional upstream- bias approximation of the Euler equations. Along all the infinite directions of wave propagation, the formulation induces anisotropic

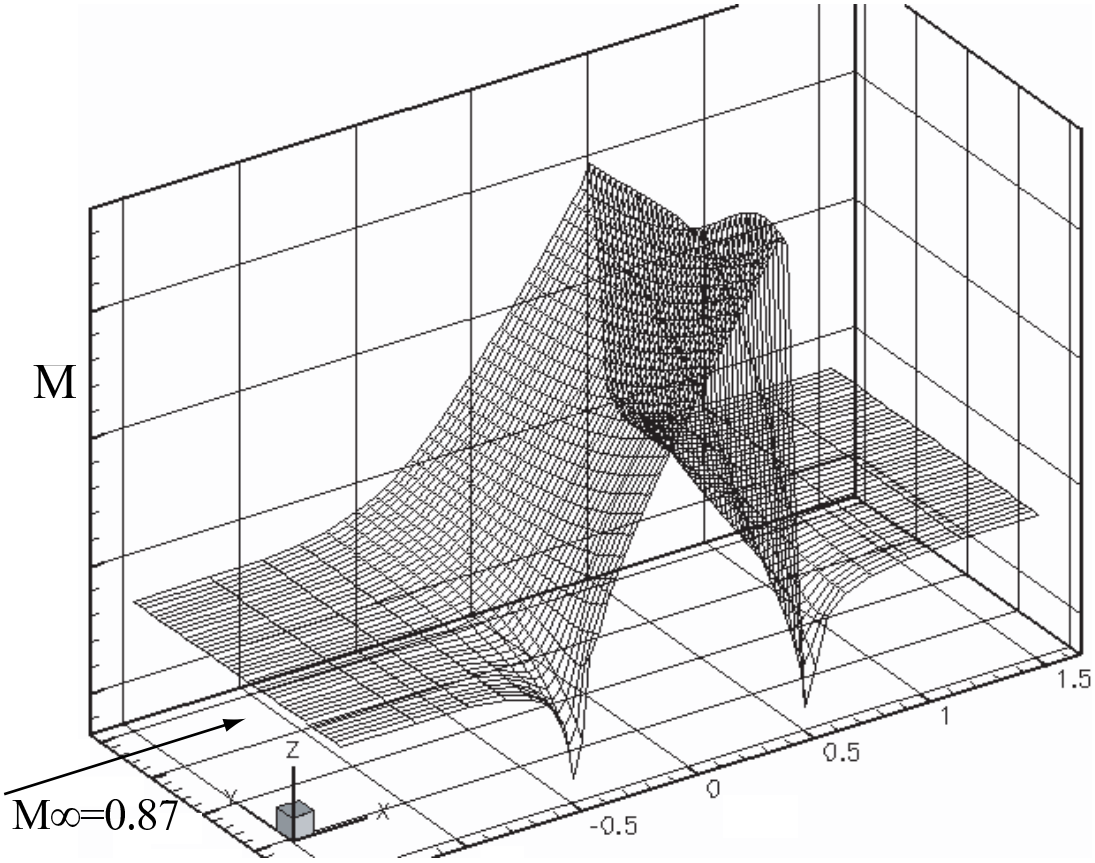

Figure 8: $M_\infty = 0.87$, Mach Number Distribution

and variable-strength consistent upwinding that correlates with the spatial distribution of characteristic velocities. The magnitude of the streamwise and crossflow upwind dissipations remain different from and independent of each other; the streamwise dissipation increases with the Mach number whereas the crossflow dissipation decreases with increasing Mach number.

The developments in this investigation have implemented the algorithm using a linear approximation of fluxes within quadrilateral cells without any MUSCL-type local extrapolation of variables. This characteristics-bias algorithm admits a straightforward implicit implementation, features a computational simplicity that parallels a traditional centered discretisation, and rationally eliminates superfluous artificial diffusion. Even on relatively coarse grids, with continuously updated upstream directions and rapid convergence to steady state, this method generates essentially non-oscillatory aerodynamic transonic-flow solutions that preserve constant total enthalpy over the flow field for adiabatic flows and mirror reference exact solutions.

REFERENCES

[1] J. Iannelli "Acoustics-Convection Upstream Resolution Algorithms for Gas Dynamic Flows", ECCOMAS 2004, (2004)

[2] J. Iannelli "A CFD Euler Solver from a Physical Acoustics-Convection Flux Jacobian Decomposition", Int. J. Numer. Meth. Fluids 31: 821-860 (1999)

[3] H. Luo, J. D. Baum, R. Löhner, J. Cabello, "Adaptive Edge-Based Finite Element Schemes for the Euler and Navier-Stokes Equations on Unstructured Grids", AIAA 93-0336 (1993).

[4] T. J. R. Hughes and A. Brooks, "A Theoretical Framework for Petrov-Galerkin Methods with Discontinuous Weighting Functions: Application to the Streamline-Upwind Procedure", Finite Elements in Fluids IV, 47-65, John Wiley, (1982).

[5] T. J. R. Hughes, "Recent Progress in the Development and Understanding of SUPG Methods with Special Reference to the Compressible Euler and Navier-Stokes Equations", International Journal for Numerical Methods in Fluids, 7, 11, (1987).

[6] C. Johnson, *Numerical Solution of Partial Differential Equations by the Finite Element Method*, Cambridge (1987).

[7] C. Johnson and Anders Szepessy, "On the Convergence of a Finite Element Method for a Nonlinear Hyperbolic Conservation Law", Mathematics of Computation, 49, 180, 427-444, (1987).

[8] C. Johnson, A. Szepessy, P. Hansbo, " On the Convergence of Shock-Capturing Streamline Diffusion Finite Element Methods for Hyperbolic Conservation Laws", Mathematics of Computation, 54, 189, 107-129, (1990).

[9] J.-C. Carette, H. Deconinck, H. Paillere, P. L. Roe, "Multidimensional Upwinding: Its Relation to Finite Elements", Inter. Journ. Numer. Meth. in Fluids, 20, 935-955, (1995).

[10] S.F. Davis, "A Rotationally-Biased Upwind Difference Scheme for the Euler Equations", Journal of Computational Physics 56, 65-92 (1984).

[11] D.W. Levy, K.G. Powell, and B. van Leer, "Use of a Rotated Riemann Solver for the Two-Dimensional Euler Equations", Journal of Computational Physics 106, 201-214 (1993).

[12] A. Dadone, and B. Grossman, "A Rotated Upwind Scheme for the Euler Equations", AIAA 91-0635 (1991).

[13] W. Coirier and B. van Leer, "Numerical Flux Formulas for the Euler and Navier-Stokes Equations: II. Progress in Flux-Vector Splitting", AIAA-91-1566, (1991).

[14] C. L. Rumsey, B. van Leer, P. L. Roe, " A Multidimensional Flux Function with Applications to the Euler and Navier-Stokes Equations" Journal of Computational Physics 105, 306-323 (1993).

[15] I. H. Parpia, "A Planar Oblique Wave Model for the Euler Equations" AIAA-91-1545-CP, (1991).

[16] H. Paillere, H. Deconinck, R. Struijs, P. L. Roe, L.M. Mesaros, J.D. Muller, "Computations of Inviscid Compressible Flows Using Fluctuation-Splitting on Triangular Meshes", AIAA 93-3301, (1993).

[17] P. L. Roe, "Beyond the Riemann Problem: Part I", in *Algorithmic Trends in CFD*, Springer Verlag (1993).

[18] C. Hirsch, *Numerical Computation of Internal and External Flows*, Vol. 1, 2 John Wiley & Sons, New York, NY, (1991).

[19] P. R. Garabedian, *Partial Differential Equations*, Chelsea Publishing Company, New York, N. Y., (1986).

[20] E. Zauderer, *Partial Differential Equations of Applied Mathematics*, John Wiley, New York, N. Y., (1989).

[21] K. Dekker and J.G. Verwer, *Stability of Runge-Kutta Methods for Stiff Non-Linear Differential Equations*, Elsevier Publishers, Amsterdam, (1984).